PERGAMON

International Journal of Heat and Mass Transfer 44 (2001) 1–15

International Journal of HEAT and MASS TRANSFER

www.elsevier.com/locate/ijhmt

Transient two-phase flow in arbitrary inclined tubes caused by depressurization of liquid with dissolved gases

S. Richter [a,*], S. Fleischer [b], M. Aritomi [a], R. Hampel [b]

[a] *Tokyo Institute of Technology, Research Laboratory for Nuclear Reactors, 2-12-1 Ohokayama, Meguro-ku, 152 Tokyo, Japan*
[b] *University of Applied Science Zittau/Goerlitz, Theodor Koerner Allee 16, 02763 Zittau, Germany*

Received 16 April 1999; received in revised form 6 March 2000

Abstract

Hydrostatic level measurement systems (HLMSs), applied to pressure vessels, loose their reliability during transient processes, if the depressurization of water that absorbed a certain amount of gases at high pressure initiates bubble formation and movement through the liquid in these systems. To simulate and predict the effect of migrating bubbles on the reliability of HLMS, a model was proposed taking bubble formation, motion and mass diffusion of dissolved multi-component gases through the supersaturated liquid into consideration. The one-dimensional flow model, which described the two-phase flow in tubes (5–10 mm) by use of Eulerian and Lagrangian coordinate systems, was applied to bubbly and slug flow through arbitrary inclined tubes without junctions. A transition criterion between the two flow regimes was defined. A homogenous nucleation model with pressure, temperature and fluid properties as parameters was developed for gas-in-liquid solions. The mass transfer rate by gas diffusion from the supersaturated liquid into the formed bubbles was calculated by numerical solution of an introduced differential equation. The quality of the proposed model was examined by the simulation of an experimental series where a binary gas–liquid solution was depressurized under variation of saturation pressure, release velocity and tubing geometry. The behavior of the water level, bubble size and velocity was observed by use of needle probes and a conductive sensor. The simulated data found confirmation by the experimentally obtained results.

1. Introduction

For many applications in nuclear and chemical industries, the fluid level in pressurized vessel has to be measured. Therefore, the hydrostatic pressure at the bottom of the vessel is compared to the pressure of a liquid column with known level (Hydrostatic Level Measurement System HLMS). For practical considerations (the usual case of approximately the same temperature in both systems and sufficient slow transients), HLMS is characterized by a linear dependency from the liquid level to the measured pressure difference. Due to its simplicity this measuring principle is used in a wide range of applications.

If the system pressure drops suddenly, that might be caused by release of an overpressure valve or by a pipe rupture, possibly dissolved gases in the liquid phase nucleate and form bubbles which are accelerated by the gravitational force and traverse through the tubing system. The interaction of formation, moving, coalescence and separation of the bubbles characterizes this process. Furthermore, a diffusion

* Corresponding author.
E-mail address: richter@2phase.nr.titech.ac.jp (S. Richter).

0017-9310/01/$ - see front matter
PII: S0017-9310(00)00100-9

Nomenclature

A	area (m^2)
c	relative velocity (m/s)
c_W	drag coefficient
D	diameter (m)
f	friction factor
K	constant
L	length (m)
m	mass (kg)
M	molar mass (kg/kmol)
n	bubble density ($1/m^3$)
N	bubble number
p	pressure (Pa)
R	radius (m)
T	temperature (°C)
u	velocity (m/s)
V	volume (m^3)
x	molar concentration (kmol/kmol)
y	coordinate normal to surface (m)
z	length coordinate (m)
Z	integral length coordinate (m)
Z_ν	real gas coefficient
$\langle\varepsilon\rangle$	area averaged void fraction
Δ	difference, general
Γ	mass flow (kg/s)
Ω	relaxation coefficient
α	tube's inclination (°)
δ	film thickness (m)
ε	volumetric void fraction
τ	time (s)
τ_i	interfacial stress (Pa)
τ_w	wall stress (Pa)
ξ	mass concentration (kg/kg)
D	diffusion constant (m^2/s)
C_H	Henry constant (Pa)
M_ν	molar mass of ν (kg/kmol)
R_ν	specific gas constant of ν (kJ/kgK)
η	dynamic viscosity (Pa s)
ν	kinematic viscosity (m^2/s)
ρ	specific weight (kg/m^3)
σ	surface tension (N/m)

Subscripts

acc	acceleration
B	bubble
C	conduit
CV	control volume
equi	equilibrium
f	friction
form	form
G	gas
H	Henry
in	added
j	present element
$j+1$	following element
$j-1$	preceding element
L	liquid
lam	laminar
LCV	liquid control volume
LG	direction from liquid into gas
max	maximum
out	removed
sphere	spherical bubble or concerning nose of a plug
T	Taylor bubble
TPCV	two-phase control volume
turb	turbulent
x	component in x
y	component in y
z	component in z
ν	gas phase 1, 2

Superscripts

$\sim$	Lagrangian coordinate
–	average
i	interface
k	present calculation step
$k+1$	next calculation step
$k-1$	former calculation step
w	wall

of the solved (multi-component) gaseous phase from the supersaturated liquid into the bubbles takes place.

It is obvious that the local pressure inside the tube alters or even an unknown volume of liquid is pushed out of the system when the expanding multi-phase mixture exceeds the limits of the facility. In any case the applicability of HLMS is lost.

So it is of practical interest to predict the behavior of a liquid column during pressure drops with the aim to use the simple principle of HLMS, but be aware of the limitations and the degree of uncertainty in the case of accidental operation.

The proposed model will be able to simulate the required information. Previous work was realized at the University of Applied Science, Zittau/Goerlitz, Germany, where depressurization tests for practically used configurations of HLMS were carried out.

2. Theoretical background

The depressurization of a saturated gas–liquid solution is governed by three mechanisms: formation of bubbles by nucleation, migration of these formed bubbles through the containing tubing system and mass transfer of the absorbed gas from the liquid into the bubbles due to concentration gradients from the saturated interface to the supersaturated liquid. These mechanisms are dependent on each other but can be formulated separately in a nucleation, a flow and a diffusion model.

2.1. Flow model

The proposed model is one-dimensional and suitable for a time-dependent simulation of bubble and slug flow in thin tubes. The liquid phase is treated as incompressible and observed through an Eulerian framework. Bubbles are modeled compressible, as migrating objects carrying their individual Lagrangian coordinate base. Since tubes of industrial applied HLMS are thin in diameter (about 8 mm), single bubbles are supposed to fill almost all of the cross sectional area so that at an observed point of the tube's length coordinate z, only one bubble can exist. So it becomes possible to distinguish between tube-zones which are only occupied with liquid, further referred as liquid control volumes (LCVs), and zones which contain either a slug or a bubble, further referred as two-phase control volumes (TPCVs).

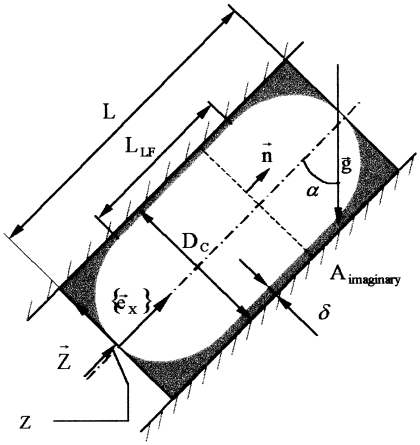

$$Z = \left(\mathbf{u}_L, \mathbf{u}_G, <\varepsilon>, \left(\frac{\partial p}{\partial z}\right)_L, \left(\frac{\partial p}{\partial z}\right)_G, \rho_L, \rho_G, \Gamma_{LG} \right)^T$$

Fig. 1. Two-phase control volume TPCV. The Lagrangian basis posed by the vector **Z** and some geometrical definitions are illustrated.

In general, control volumes are defined as a tube section limited by the wall surface and two parallel planes as illustrated in Fig. 1.

From Fig. 1, it can be seen that the normal vector of these planes have the direction of the length coordinate z. At the position of the lowest z-value, a Lagrangian coordinate system $\{e_z\}$ is defined. This coordinate base includes, apart from the spatial coordinate, information about volumetric- and sectional cross-averaged properties of the CV (ε, ρ_L, ρ_G, υ_L, u_G, L, Γ_{LG}, F_R^i, F_R^w, $\partial p_{(L)}/\partial z$, $\partial p_{(G)}/\partial z$) concentrated in the property vector **Z**.

Furthermore, an imaginary plane, which may have an arbitrary position between the z-values of the planes defining the CV, is introduced. This introduction is necessary for numerical purpose: the demand to simulate tubing systems without junctions but with sectors of different inclinations yields that a moved control volume has to pass these transition points between one and another tubing-sector. It directly follows that two components of the gravational force act on different parts of one control volume. By use of the imaginary plane, which is fixed in the point of the geometrical singularity, the original control volume is divided into two pseudo-control volumes. In each of them the gravity force is constant and the equation of conservation can be integrated separately. Generally, there is the possibility to define more than one of such planes and integrate over the resulting pseudo-control volumes. This is necessary if a very long control volume occupies more than one point of geometrical singularity. The usefulness in the case of long plugs is the object of further investigation. For the present calculation such bubbles never appeared.

2.1.1. Equations of conservation

The equations of conservation were derived under the assumption of an isothermal process. The set reduces to the balances of mass and momentum for each phase. Similar equations are referred to [1,3–5]. The equations of conservation are defined separately for each type of control volume. Each phase is balanced.

Assumptions were made as follows: the density of the phases and the void fraction are volume-averaged; the pressure is averaged over the cross section but varies over the length coordinate z. The cross section is considered as no function of z (i.e., constant diameter). The influence of mass transfer (diffusion from dissolved gases into the bubble) is only reflected in the equation of momentum conservation, not in the equation of mass conservation.

Equation of mass conservation for LCV:

$$\frac{\partial L}{\partial \tau} + \frac{\partial}{\partial z}[u_L L] = 0 \tag{1}$$

Equation of momentum conservation for LCV:

$$\frac{\partial}{\partial\tau}[u_L L]+\frac{\partial}{\partial z}[u_L u_L L]+\frac{L}{\rho_L}\frac{\partial p_{L,f}}{\partial z}+Lg\sin\alpha=0 \tag{2}$$

Equation of mass conservation for the gaseous phase of TPCV:

$$\frac{\partial}{\partial\tau}\left[\varepsilon\rho_G L\right]+\frac{\partial}{\partial z}\left[\varepsilon\rho_G u_G L\right]+\frac{\Gamma_{LG}}{A_c}=0 \tag{3}$$

Equation for mass conservation for the liquid phase of TPCV:

$$\frac{\partial}{\partial\tau}\left[(1-\varepsilon)\rho_L L\right]+\frac{\partial}{\partial z}\left[(1-\varepsilon)\rho_L u_L L\right]-\frac{\Gamma_{LG}}{A_c}=0 \tag{4}$$

Equation of momentum conservation for the gaseous phase of TPCV:

$$\begin{aligned}&\frac{\partial}{\partial\tau}\left[\varepsilon\rho_G u_G L\right]+\frac{\partial}{\partial z}\left[\varepsilon\rho_G u_G u_G L\right]+\varepsilon L\frac{\partial p_{(G)}}{\partial z}\\&\quad+\varepsilon\rho_G Lg\sin\alpha+\frac{F^{i}_{f,LF}}{A_c}+\frac{\Gamma_{LG}}{A_c}(u_L-u_G)=0\end{aligned} \tag{5}$$

Equation of momentum conservation for the liquid phase of TPCV:

$$\begin{aligned}&\frac{\partial}{\partial\tau}\left[(1-\varepsilon)\rho_L u_L L\right]+\frac{\partial}{\partial z}\left[(1-\varepsilon)\rho_L u_L u_L L\right]\\&\quad+(1-\varepsilon)L_G\frac{\partial p_{(L)}}{\partial z}\quad+(1-\varepsilon)\rho_L Lg\sin\alpha\\&\quad-\frac{F^{i}_{f,LF}}{A_c}+\frac{F^{W}_{f,LF}}{A_c}-\frac{\Gamma_{LG}}{A_c}(u_L-u_G)-\frac{F_{drag-sphere}}{A_c}=0\end{aligned} \tag{6}$$

It is noteworthy that the equations of mass conservation are obtained by volume averaging (and so describing the integral behavior of the control volume), but the equations of momentum conservation are based on averaging over the cross section. So it became possible to implement distinctive pressure loss models.

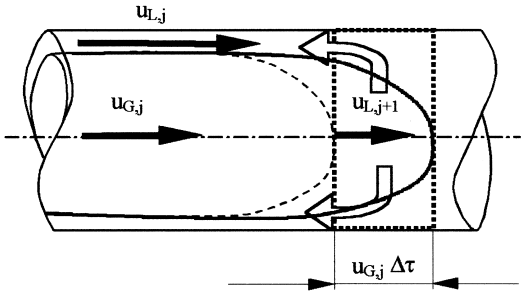

Fig. 2. A traversing plug displaces liquid with a relative velocity of $u_{Lj+1}-u_{Gj}$.

The set of equations is also characterized by dependencies among variables of interfacial force F_{Ri}, mass exchange between the phases Γ_{LG} and pressure gradient in the liquid phase $\partial p_L/\partial z$.

If it is taken into consideration that alternating types of CVs represent the whole column, it is possible to show that a moving bubble displaces a specific volume of liquid per unit time as illustrated in Fig. 2. The dependency between the rising velocity of the bubble, its void fraction and the velocity of the liquid can be correlated. This results in an enormous simplification of the set of differential equations:

$$u_{I,j}=\frac{u_{L,j+1}-\langle\varepsilon\rangle_j u_{G,j}}{1-\langle\varepsilon\rangle_j}\approx\frac{u_{L,j+1}-u_{G,j}}{1-\langle\varepsilon\rangle_j}\approx\frac{u_{G,j}}{1-\langle\varepsilon\rangle_j} \tag{7}$$

In view of this, a momentum balance is reached by combination of Eqs. (5) and (6) and by use of the kinematic correlation (7) representing the dynamic behavior of both phases for high volumetric void fraction in a TPCV and near stagnant fluid flow. The obtained Eq. (8) is based on the velocity of the gaseous phase. This is of particular interest for implementation, because from the solution of Eq. (8) the velocity of the liquid phase can be calculated directly by use of the kinematic correlation (7). The combined equation of momentum conservation for a TPCV can be written in discreet form:

$$\begin{aligned}u^{k+1}_{G,j}:=&\left[m^{k}_{G,j}u^{k}_{G,j}-\frac{m^{k}_{G,j}}{\rho^{k}_{G,j}}\left(\frac{\partial p_{L,f}}{\partial z}\right)^{k}_{j}\right.\\&\left.+m^{k}_{G,j}\left(1-\frac{\rho_L}{\rho^{k}_{G,j}}\right)g\sin\alpha\right]\Delta\tau\frac{K^{k}_{Dyn}}{m^{k+1}_{G,j}}\\&-\left[\left(F^{i}_{f}\right)^{k}_{j}+\Gamma^{k}_{LGj}\left(u^{k}_{G,j}-u^{-1}_{L,j}\right)+F^{k}_{Dragj}\right]\Delta\tau\frac{K^{k}_{Dyn}}{m^{k+1}_{G,j}}\end{aligned} \tag{8}$$

where

$$m^{k}_{G,j}:=\rho^{k}_{G,j}\left[\iiint_{(V_G)}\mathrm{d}V\right]^{k}_{j}; \tag{9a}$$

The dynamic coefficient K_{Dyn}, used in Eq. (8), can be obtained, if the equations of momentum conservation of gaseous (5) and liquid phase (6) are compared and terms of lower order are neglected. The ratio of the so reached expression differs from Eq. (5) by a constant factor. This coefficient is expressed by Eq. (11) and might be understood as the ratio between the reaction on a defined force by an independent gaseous phase compared to the reaction on the same force by the kinematic coupled two-phase mixture inside the TPCV.

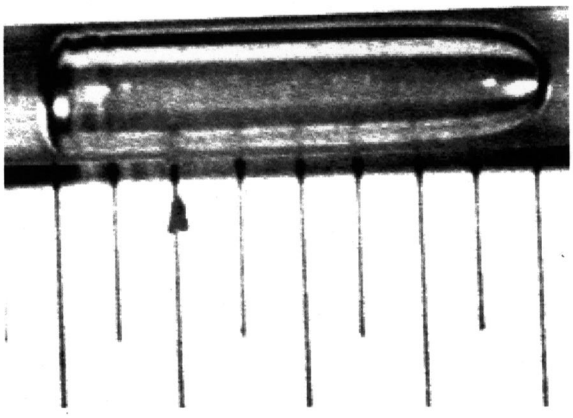

Fig. 3. Air plug inside a 8 mm, 45° inclined, water filled tube ($T = 20°C$, $p = 1$ bar, $u \cong 8$ cm/s).

$$K_{\mathrm{Dyn}}: = \frac{\varepsilon_j^k \rho_{\mathrm{G},\,j}^k}{\rho_{\mathrm{L}}} \tag{9b}$$

The obtained set of equations is characterized by 5 (LCV) and 11 (TPCV) unknown variables, whereas 2 (LCV) and 4 (TPCV) balance equations are available. In the following section constitutive equations will be proposed to close the problem.

2.1.2. Constitutive equations

The set of constitutive equations is derived separately for three different flow regimes: liquid single-phase flow as well as two-phase flow with bubbles or plugs.

It is assumed that the bubbles have a spherical shape, while plugs have a cylindrical body set between two half spheres. The "classical" shape of elongated Taylor bubbles, characterized by a spherical cap nose and abruptly termination, could not be observed. Bubbles showed much more tendency towards two spherical caps, what is caused by a significant stronger influence of the surface tension on the bubble shape in tubes of small radius. The gaseous phase is supposed to flow concentric through the tube. (More complicated two-dimensional approaches taking eccentric flow into consideration gave similar results.)

These geometrical assumptions are basis for any calculation. They were confirmed by observation with a CCD camera as illustrated in Figs. 3 and 4.

The liquid in LCVs is accelerated by the formation and the growing of bubbles. The volume expansion of existing bubbles is a result of pressure decrease during the transient release process as well as mass transfer from dissolved gases into the bubble. The experimentally maximum observed Reynolds Number was in the order of 10 which legitimizes the laminar approach:

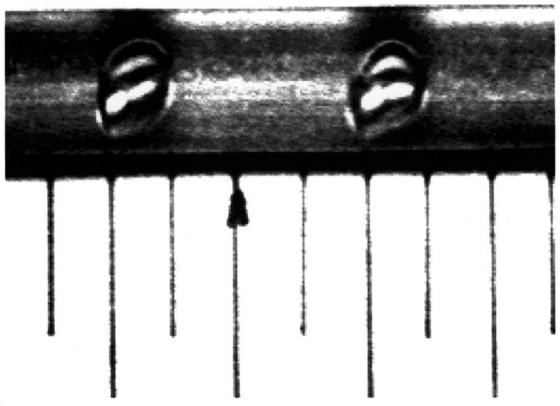

Fig. 4. Air bubbles in a 8 mm, 45° inclined, water filled tube ($T = 20°C$, $p = 1$ bar, $u \cong 10$ cm/s).

$$\frac{\partial p_{\mathrm{L,\,f}}}{\partial z} = \frac{64}{Re}\frac{\rho_{\mathrm{L}}}{2}u_{\mathrm{L}}^2\frac{1}{D_{\mathrm{c}}} = \frac{32\nu_{\mathrm{L}}\rho_{\mathrm{L}}u_{\mathrm{L}}}{D_2^2} \tag{10}$$

The equations of conservation can be solved by use of this constitutive equation. To obtain the constitutive equations for a TPCV, it is necessary to distinguish between bubbly and plug flow due to their different geometrical appearance. However, certain general definitions can be made:

Cross sectional averaged void fraction:

$$\langle\varepsilon\rangle = \frac{D_{\mathrm{G}}^2}{D_{\mathrm{c}}^2} \tag{11}$$

Volume averaged void fraction:

$$\varepsilon = \frac{1}{V_{\mathrm{TPCV}}}\iiint_{(\mathrm{TPCV})}\mathrm{d}V_{\mathrm{G}} \tag{12}$$

Finally, three velocities are defined: superseding, volume averaged and maximum liquid velocity:

$$c_j = (u_{\mathrm{G},\,j} - u_{\mathrm{L},\,j+1}) \tag{13}$$

$$u_{\mathrm{L}} = -\frac{c}{1-\varepsilon} \tag{14}$$

$$u_{\mathrm{L,\,max}} = -\frac{c}{1-\langle\varepsilon\rangle_{\max}} \tag{15}$$

According to Fig. 5, an equation for the pressure gradient is derived that acts on the complementary phase.[1]

[1] This becomes obviously by calculation of local pressure and neglecting the dynamic forces; $p(z) = p_0 - \int_z \rho_{\mathrm{L}} g \sin\alpha\,\mathrm{d}z - \frac{\rho_{\mathrm{L}}}{2}u_{\mathrm{L}}^2 + \int\frac{\partial p_{\mathrm{L,\,f}}}{\partial z}\mathrm{d}z$.

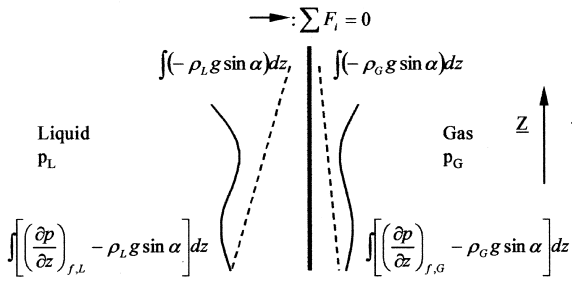

Fig. 5. Force balance at a non-accelerated interface with negligible mass exchange in a general formulation (neglecting of the influence of surface tension).

$$\frac{\partial p_{(\mathrm{L})}}{\partial z} = \frac{\partial p_{\mathrm{G,\,f}}}{\partial z} - g\rho_{\mathrm{G}}\sin\alpha \tag{16}$$

$$\frac{\partial p_{(\mathrm{G})}}{\partial z} = \frac{\partial p_{\mathrm{L,\,f}}}{\partial z} - g\rho_{\mathrm{L}}\sin\alpha \tag{17}$$

The pressure loss resulting by non-ideal acceleration of the liquid around the bubble is calculated by:

$$\left(\frac{\partial p}{\partial z}\right)_{\mathrm{acc}} = K_{\mathrm{acc}}\frac{\rho_{\mathrm{L}}}{2}(u_{\mathrm{L},\,j+1} - u_{\mathrm{L},\,j})|u_{\mathrm{L},\,j+1} - u_{\mathrm{L},\,j}|\frac{1}{L} \tag{18}$$

The coefficient K_{acc} was empirically determined and has a value of 0.480 in the case of bubbly and 0.525 in the case of plug flow. For bubbly flow, the drag force on a spherical bubble is calculated with conventional equations approximating the drag coefficient diagrams for a sphere and are given by Eq. (21).

During the sparkling experiments, described in detail in Section 3, it was observed that the liquid passes the bubble without remarkable wave formation in the liquid film. Based on this observation, a laminar approach for the pressure loss in the liquid phase was made and writes as Eq. (22):

$$\frac{\partial p_{\mathrm{G,\,f}}}{\partial z} = c_{\mathrm{w}}\frac{\pi}{8}D_{\mathrm{G}}^2\rho_{\mathrm{L}}c^2\frac{1}{\pi D_{\mathrm{c}}^2 L} \tag{19}$$

$$\frac{\partial p_{\mathrm{L,\,f}}}{\partial z} = 2f_{\mathrm{f}}\frac{\dot{m}}{D_{\mathrm{G}}\rho_{\mathrm{L}}} = 2f_{\mathrm{f}}\frac{u_{\mathrm{L}}^2\rho_{\mathrm{L}}}{D_{\mathrm{G}}} \tag{20}$$

with

$$c_{\mathrm{w}} = \begin{cases} Re \le 0.5: & \dfrac{24}{Re} \\ 0.5 < Re \le 1000: & 0.4 + \dfrac{24}{Re} + \dfrac{24}{Re^2} \\ 1000 < Re \le 10{,}000: & 0.42 \\ 1000 < Re: & 0.13 \end{cases} \tag{21}$$

$$f_{\mathrm{f}} = \frac{16}{Re} \tag{22}$$

The methodology for finding closing relationships in the case of plug flow is similar to the TPCV applied to bubbly flow. Difference is that the drag coefficient for the plug nose is assumed as constant (0.2). Similarly in the case of bubbly flow, it was experimentally observed that the film did not show remarkable protuberances in form of surface waves on the interface. Insofar the assumption of laminar flow was extended to plug flow. For the calculation of the pressure loss in the liquid film a laminar film theory was developed as shown in the following: in general, the pressure loss can be calculated by balancing the forces, acting on a liquid film [2]:

$$\left(\frac{\partial p}{\partial z}\right)_{\mathrm{f}} = \frac{(\tau^{\mathrm{i}} - \tau^{\mathrm{w}})P_{\mathrm{T}}}{A_{\mathrm{c}}}\frac{L_{\mathrm{LF}}}{L} - \rho_{\mathrm{L}}g\sin\alpha \tag{23}$$

In Eq. (23), the length of the liquid film (cylindrical part) as well as the shear stress at the wall and on the interface are unknown. In the case of laminar flow, the shear stress behaves linear over the film thickness. This offers an approach given by:

$$\tau(y) = C_1 y + C_2 = \eta_{\mathrm{lam}}\frac{\partial u_{\mathrm{z}}}{\partial y} \tag{24}$$

Eq. (24) is integrated. Boundaries are defined by no-slip condition at the wall and the interface and the continuity of mass according to Eq. (7). As a result, the shear stresses at the surface of bubble and wall as well as the film thickness are obtained.

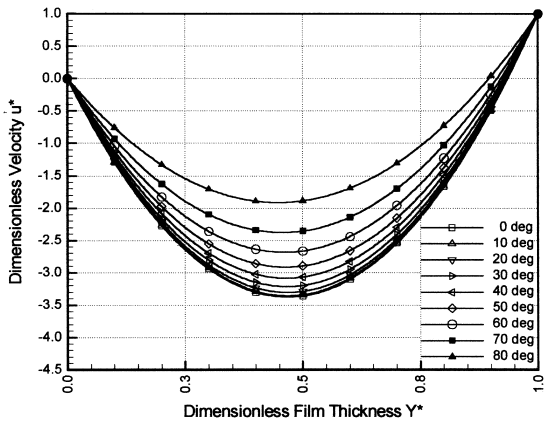

Fig. 6. Dimensionless velocity profiles as a function of tube inclination and a dimensionless film thickness for a laminar liquid film.

$$\tau^{w} = \tau(y=0) = \eta_{lam}\frac{u_G}{\delta}\left[1 - \frac{3}{\delta}\left(\frac{D_c}{2} + \delta\right)\right] \quad (25)$$

$$\tau^{i} = \tau(y=\delta) = \eta_{lam}\frac{u_G}{\delta}\left[1 + \frac{3}{\delta}\left(\frac{D_c}{2} + \delta\right)\right] \quad (26)$$

$$0 = (\delta_j)^3 - 6\frac{u_{G,j}\nu_L}{g\sin\alpha}\delta_j - 3\frac{u_{G,j}\nu_L D_c}{g\sin\alpha} \quad (27)$$

For illustration, a plot of velocities simulated for different tube inclinations is added in Fig. 6. The plot requires Eq. (28), which allows to conclude the velocity distribution:

$$u(y) = \left[\frac{3u_G}{\delta^3}\left(\frac{D_c}{2} + \delta\right)\right]y^2 + \frac{u_G}{\delta}\left[1 - \frac{3}{\delta}\left(\frac{D_c}{2} + \delta\right)\right]y \quad (28)$$

Since bubbles are expanding as result of pressure decrease and gas diffusion into the bubble, there is a requirement to define a transition criterion between bubbly and plug flow: it is assumed that the transition takes place, if the possibility for the existence of a stable laminar film occurs.

$$\delta(u_G) > \frac{1}{2}(D_c - D_G) \quad (29)$$

The reached results were able to represent the experimental data.

2.2. Diffusion model

HLMSs consist of a stagnant liquid column. This liquid possibly contains solved gases, which were absorbed from the surrounding at high pressure during a long period of time. If, as an effect of a sudden drop in the system pressure, it falls a certain degree below the saturation pressure corresponding to the amount of absorbed gas, bubbles nucleate and the liquid will be supersaturated since the nucleation process demands a specific non-equilibrium state of the solution. The partial pressure of the gas component in the gas–liquid interface will be naturally corresponding to the pressure inside the bubble. The local difference of the gas mass concentration from the interface to a point in the liquid, yields a diffusion mass flux which influences the gas mass in the bubble.

This diffusion takes place in a complicated three-dimensional flow field of the liquid. There is necessity of simplification to apply numerical treatment and therefore the following assumptions are made: the bubble shape follows the geometrical assumptions made for the flow model. Due to concentric flow of a bubble, a two-dimensional simulation of the local gas mass concentration in the liquid phase is sufficient. Mass transfer at the noses of a slug is neglected, because the area is comparatively small, yielding a very small absolute mass flow. So, only the mass transfer over the cylindrical part of the interface was taken into consideration. In this film region the velocity profile of the liquid is given by Eq. (28). In the case of spherical bubbles, mass transfer by diffusion, is generally neglected. Paying respect to the mass transfer into spherical bubbles did not show significant differences in the behavior of the water level but increased the computational time enormously. A final assumption has to be made for the time dependence of the solution: if the liquid, that is displaced by a migrating bubble, enters the film in the cylindrical wall region the gas mass concentration is supposed to be homogenous over the cross section (ideal mixing takes place in the LCV). As a consequence of gas diffusion, the concentration profile changes over the length coordinate what yields that at the beginning the diffusion mass flux will be higher than at the end of a plug. In general, as higher as the sectional cross-averaged liquid velocity in the film region is, as higher is the transferred mass flux and as more homogenous is the gas mass concentration profile at the end of the liquid film zone. The cause is that the velocity gradients on the interface are higher and the time the liquid flows in the film region is shorter. If it is taken into consideration that a new nucleated bubble accelerates but does not further experience sudden changes in the rising velocity, a time independent simulation is valid.

With the above mentioned assumptions, an equation of gas mass conservation as well as boundary conditions for its solution can be formulated according to Fig. 7.

Steady state mass balance for each gas component v:

$$u(y)\frac{\partial \xi_{G,v}}{\partial x} + D_{LG,v}\left(\frac{\partial^2 \xi_{G,v}}{\partial y^2} + \frac{\partial^2 \xi_{G,v}}{\partial x^2}\right) = 0 \quad (30)$$

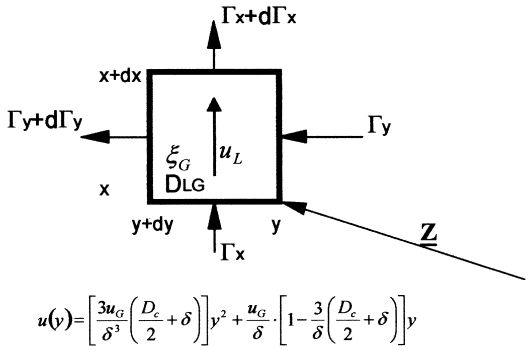

Fig. 7. Segment of the laminar liquid film. Basis for the derivation of a mass balance for each gas component.

requiring the following boundary conditions:

$$\xi_{G,\nu}(x = L_G, y) = \xi_{G,\nu,j+1} \tag{31}$$

$$\xi_{G,\nu}(x, y = \delta) = \xi_{\text{equi},\nu}(p_G, T) \tag{32}$$

$$\frac{\partial \xi_{G,\nu}(x, y = 0)}{\partial y} = 0 \tag{33}$$

$$\frac{\partial \xi_{G,\nu}(x = 0, y)}{\partial x} = \frac{\partial \xi_{G,\nu}(x = \mathrm{d}x, y)}{\partial x} \tag{34}$$

The mass concentration at the equilibrium is calculated by the law of Henry. Here the pressure increase due to the acting of surface tension was taken into consideration:

$$x_{\nu,\text{equi}} = \frac{x_\nu \left(p_L + \frac{4\sigma}{D_B}\right)}{K_{H,\nu}(T)} \tag{35}$$

The molar concentration x can be converted into the mass concentration ξ:

$$\xi_\nu = \frac{x_\nu M_\nu}{\sum_{j=1}^{N} x_j M_j} \tag{36}$$

The concentration profiles are solved for each bubble at each global time step numerically. After convergence is reached the diffusion mass transfer can be integrated:

$$\Gamma_{LG,\nu} = P_c \rho_L \int_{y=0}^{\delta} u(y)\left[\xi_{\nu,j+1} - \xi_\nu(y)_{x=0}\right] \mathrm{d}y \tag{37}$$

2.3. Nucleation model

During pressure release in the HLMS, the partial pressure of the dissolved gases decreases proportional to the system pressure but the mass of the gas in the solution is constant. If the system pressure drops below a certain value, the partial pressure of the gas (or one component of it) will be higher than the saturation pressure. The result is chemical non-equilibrium, which might form a special degree or possibly cause bubble formation. The mechanical structure of the HLMS is considered as very complex so that there is no information concerning the surface structure of tubes or possible gas cavities in connectors. That is why the proposed approach is based on the assumption that there is no preferred place for nucleation sites. The model is based on homogenous nucleation (a possible underestimation of the pressure during a transient where first bubbles occur did not found experimental verification as pointed out later).

The work for the formation of a single bubble is available in the form of chemical energy by a partial pressure that is higher than the saturation pressure. This work is supposed to be equivalent to the negative work required for the formation of a bubble and governed by the action of surface tension [5]:

Work to form a spherical bubble of radius r_B:

$$\Delta W_B = -4\pi r_B^2 \sigma \tag{38}$$

Work available by dissolution of a sphere with radius r_B:

$$\Delta W_L = \frac{4}{3}\pi r_B^3 (p_{i,L} - p_{i,L,\text{equi}}) \tag{39}$$

Comparison of these two equations yields the radius. In the case of a two component gas it writes as follows:

$$r_{B,\nu} = \frac{3\sigma}{p_L}\left(K_{\text{grad}}\xi_\nu \frac{1}{M_\nu\left(\frac{\xi_1}{M_1} + \frac{\xi_2}{M_2} + \frac{(1-\xi_2-\xi_2)}{M_L}\right)} - x_\nu \frac{p_L}{K_{H,\nu}}\right)^{-1}$$

$$\nu \in 1, 2 \tag{40}$$

The coefficient K_{grad} was added to pay attention to the form of concentration gradients in the liquid phase, similar to the introduction of a Biot number for heat transfer problems: the idea is to increase the dissolved volume artificially to take the amount of gas, which is dissolved by the concentration gradients in

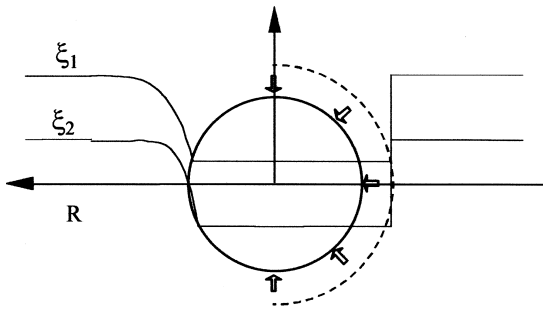

Fig. 8. Illustration for the introduction of a coefficient, which takes the dissolved gas due to gradients in the concentration field into consideration.

the liquid phase, into consideration. An illustration is given in Fig. 8. The problem is simplified to a calculation with two discreet concentration levels.

Furthermore, there is necessity to specify the number of bubbles, which exist in dispersed form in a predefined environment [4]. If it is considered that the numbers of nucleation sites n_B (and so the corresponding void fraction ε for standard conditions) is well known, it can be extrapolated to arbitrary conditions if real gas properties are neglected:

$$\varepsilon = \varepsilon_0 \frac{p_0 T}{p T_0} \tag{41}$$

With the assumption of spherical bubbles it follows from Eq. (40):

$$n_{B,\nu} = \varepsilon_0 \frac{p_{0,L}}{p_L} \frac{T_L}{T_{0,L}} \frac{3}{4\pi} \times \left[\frac{3\sigma}{p_L} \left[K_{grad} \xi_\nu \frac{1}{M_\nu \left(\frac{\xi_1}{M_1} + \frac{\xi_2}{M_2} + \frac{(1-\xi_1-\xi_2)}{M_L} \right)} - x_\nu \frac{p_L}{K_{H,\nu}} \right]^{-1} \right]^{-3} \quad \nu \in 1,2 \tag{42}$$

A typical simulation of the number of nucleation sites is given in Fig. 9. It can be seen clearly that the system pressure has to fall significantly under the saturation pressure before first nucleation occurs. Further pressure decrease causes in a rapid increase of nucleation sites with almost constant radius of the formed bubble. This can be evaluated from Eq. (40). From Eq. (38) it can be seen that the available work is proportional to the pressure difference from the partial to the saturation pressure as well as to r_B^3. The work for bubble formation is proportional to the square of the radius. This yields that the radius increases with increasing pressure difference hyperbolically. So it becomes obviously that a huge difference between the partial and the saturation pressure results in less nucleation sites but bubbles with a bigger radius where a smaller difference in pressure forms a higher number of bubbles with small radius. This is reflected in the maximums of the curves in Fig. 9.

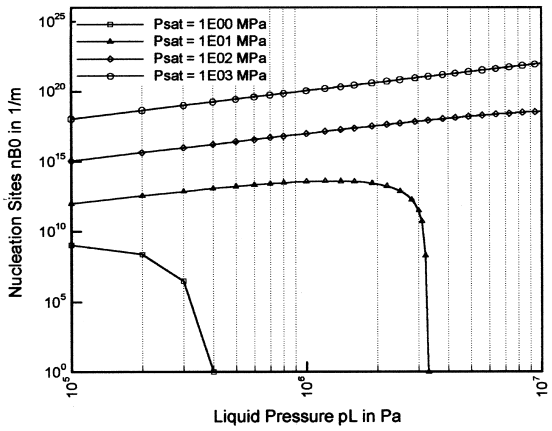

Fig. 9. Nucleation sites for a solution of nitrogen N_2 in water with the saturation pressure as parameter $T = 325$ K. $K_{grad} = 3$.

3. Experimental verification

3.1. Sparkling experiments

In the first series of experiments, the rising velocity of spherical bubbles and plugs in pipes of different inclination was investigated. An overview of the used test facility is given in Fig. 10. The apparatus consists of a storage tank (5) which was filled with degassed water at ambient temperature (20°C). The test tube (9) was flooded by use of the speed controlled pump (6). After a pre-defined level had been reached, the shut-off valve (7) was closed and the air supply started. The air compressor (1) pressurized the container (2) to damp pressure fluctuations. The supplied pressure from the container was reduced by the pressure control valve (3) to adjust a suitable pressure upstream the control valve (4) which controlled the gas flow rate into the mixing chamber (8). The mixing chamber consists of an injection needle which is concentrically arranged in the test tube. This needle has an inner diameter of 2 mm. The observation of bubbles was carried out by use of the CCD camera (11). Obtained data were

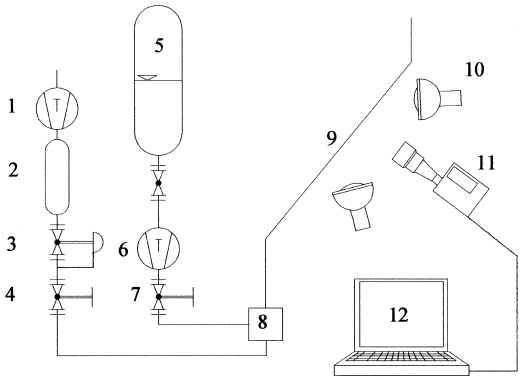

Fig. 10. Equipment of the sparkling experiments.

directly transferred to the data processing unit (12). Stroboscopes (10) were used to improve the quality of pictures. Data processing was carried out automatically on a PC. A pattern, that defines the length scale and was photographed before the experiments, was used for comparison between the defined length scale and the pictures of the bubbles recorded by the CCD camera (11). The local velocity was calculated by division of the local-instantaneous measured positions of the bubble nose and the time difference between two frames.

Single as well as collective bubbles were investigated. The bubbles had a range in diameter/length from 1 to 20. The tube was inclined at 15°, 30°, 45°, 52° and 90° (measured form the horizontal line, according to Fig. 1).

The obtained results as well as the theoretical predictions are plotted in Table 1.

From Table 1, it can be seen that the rising velocities are in the order of 10 cm/s. They are strongly dependent on the inclination angle of the tube and so the effect of the gravitational force. In more inclined tubes, bubbles migrate with slower rising velocity than in tubes closer to the vertical line. There is a tendency for a sinusoidal influence of the inclination angle to the rising velocity. This tendency is similar for any bubble length and finds a logic explanation by Eq. (2). However, an exception was observed in the case of spherical bubbles rising in a vertical tube. Here the reached velocities were slightly lower than for tubes that were inclined certain degrees. The reason was found in strong oscillations the bubbles showed. This oscillations caused huge deformations of the surface and so a higher resistance. This effect disappeared at higher inclination angles and was only observed on spherical bubbles. Detailed studies on the mechanism as well as its simulation is the object of further investigation.

Beside the influence of the inclination angle, the bubble length strongly alters the rising velocity. At a diameter/length ratio of about 2, a significant minimum in the rising velocities was observed, independent from the inclination angle. Smaller spherical as well as larger elongated bubbles showed an increase in the rising velocity.

Particularly the increase in the terminal velocity of elongated bubbles is noteworthy. The mechanism can be explained as follows: the geometric model for an elongated bubble is a cylindrical body with two spherical shaped caps. This yields Eq. (43) for the cell's volumetric void fraction:

$$\varepsilon = \varepsilon_{\mathrm{T}} = \frac{D_{\mathrm{G}}^2}{D_{\mathrm{c}}^2}\left[1 - \frac{1}{3}\frac{D_{\mathrm{G}}}{L}\right] \tag{43}$$

Eq. (43) is substituted in Eq. (5), which is written for a steady state case:

$$0 = \frac{\partial}{\partial z}[\rho_{\mathrm{G}} u_{\mathrm{G}} u_{\mathrm{G}}] + \frac{\partial p_{\mathrm{f,\,L}}}{\partial z} + \frac{1}{\dfrac{D_{\mathrm{G}}^2}{D_{\mathrm{c}}^2}\left[1 - \dfrac{1}{3}\dfrac{D_{\mathrm{G}}}{L}\right]}\left[\frac{F_{\mathrm{f,\,LF}}^{\mathrm{i}}}{LA_{\mathrm{c}}} + \frac{\Gamma_{\mathrm{LG}}}{A_{\mathrm{c}}L}(u_{\mathrm{L}} - u_{\mathrm{G}})\right] - (\rho_{\mathrm{L}} - \rho_{\mathrm{G}})g\sin\alpha \tag{44}$$

With Eq. (44), it becomes obvious that a larger bubble length L results in reduction of the third term on the left-hand side representing the effect of the resistance by friction and mass exchange. The limit of this term for $L \to \infty$ is finite and so also the rising velocity seeks a maximum for a large value of L.

Table 1 also gives an overview of the rising velocities which were numerically predicted. The simulations were confirmed by the experimentally reached data. There is an average deviation of about 5% between ex-

Table 1
Comparison of experimental reached (EXP) and simulated (SIM) rising velocities as a function of bubble length and pipe inclination[a]

LCV (mm)	15°		30°		45°		52°		90°	
	EXP (cm/s)	SIM (cm/s)	EXP (cm/s)	SIM (cm/s)	EXP (cm/s)	SIM (cm/s)	EXP (cm/s)	SIM (cm/s)	EXP (cm/s)	SIM (cm/s)
5 (Bubble)	5.4	5.3	8.5	7.6	10.0	9.5	9.8	9.7	9.0	10.1
15 (Slug)	4.0	4.2	5.0	5.2	6.0	5.7	6.0	5.8	5.0	6.1
30 (Slug)	5.0	4.9	6.8	6.7	7.3	7.7	8.9	8.1	9.0	8.7
130 (Slug)	5.0	5.4	8.0	8.5	11.0	11.3	13.0	12.2	13.0	14.0

[a] p = 1 bar, T = 20°C and D_{i} = 8 mm.

perimental and predicted data. Larger differences were observed for spherical bubbles in tubes with low inclination angle. However, the authors have the opinion that the reason is the surface deformation mentioned before.

3.2. Depressurization experiments

In the second series of experiments, the behavior of a geometrically simplified HLMS during a release of the system pressure was investigated. The media were water and air. The aim was to obtain information about the course of the water level, the nucleation pressure as well as occurring bubble sizes and rising velocities.

The used apparatus, illustrated in Fig. 11, consists of an inclined stainless steel test tube (9) with 8 mm inner diameter and a length of 2000 mm. The tube is equipped with a conductive sensor (5), which is applied at the tube wall and able to detect gas accumulations in the tube's cross-section. Parallel to the test tube, there is the bypass line (10) installed. Before the experiments, this tube had been filled with degassed water to measure the difference pressure in the test tube (9) by the differential pressure transducer (2). The system pressure is measured by the pressure transducer (3). The position of the water level as well as the rising velocity of bubbles was observed by the inductive needle probes which are installed in a 1000 mm vertical extension of the testing tube. The electrical output of these probes (4) as well as of the inductive sensor (5) were transformed by the signal converter (20) and directly transferred in the PC (21). For the experiments water had to be enriched with air. Therefore, the enrichment apparatus (15) was uncoupled from the test tube (9) by closing the three-way-valves (70) and (14). The apparatus consists of a pressurized steel container of sufficient volume, which has connectors for air and water supply. In the inner, a pipe with mesh screens have been installed which is able to disperse supplied water into drops with a size of a fraction of a millimeter. The container is half-filled with water. By use of the air compressor unit (17), the pressure inside the container was set to the aimed saturation pressure. This process was controlled by the pressure control valve (18) and the control valve (19). The water inside the enrichment apparatus was circulated by the gear pump (6). The gas-mixture was dissolved in the water since water was continuously dispersed so that air could diffuse inside the micro drops. After collecting at the container bottom, it was re-circulated. The mass concentration of oxygen was monitored by the membrane-sensor (1). This sensor demands a constant mass flow, which was realized by the flow regulating valve (16). By this procedure saturation pressure of 30, 50 and 70 bar have been realized. The corresponding dissolved gas mass concentrations were monitored by the instrument (1). This way of enrichment was chosen due to its reliability and simplicity. However, it cannot avoid the smallest non-dissolvable gas bubbles remaining in the liquid. These gas cavities were too small to be detected either by the inductive sensor (5) or by the needle probes (4). The fact that the amount of gas which was released by the liquid during the pressure transient was more than the whole amount the water could theoretically contain have drawn the authors' attention. To determine the amount of non-dissolved gas, the liquid was carefully and slowly expanded to a pressure still high compared to the nucleation pressure. During this process eventually nucleating bubbles were monitored by the inductive-sensor but could not be determined. The needle probes observed the water level. With the assumption of ideal gas behavior and by neglecting of surface tension effects, the amount of gas could be calculated from the expansion of the column, measured by the needle probes, and the system pressure which was monitored by a pressure transducer. The results of this investigation are given in Table 2.

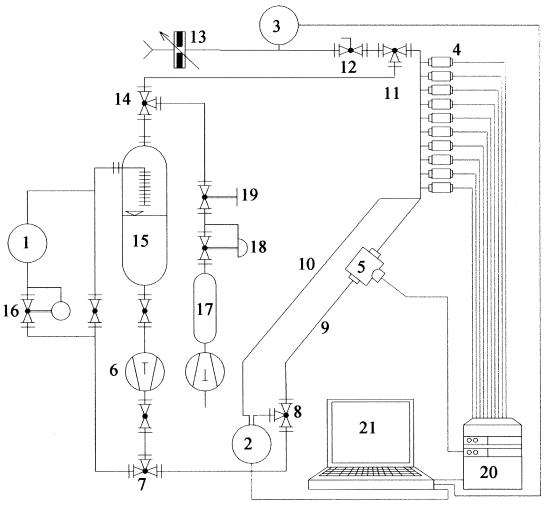

Fig. 11. Equipment of the depressurization experiments.

After the aimed concentration level of dissolved gas had been detected, the test tube was pressurized with air from the compressor unit (17) by switching the three-way-valve (14). This was necessary to avoid uncontrolled bubble formation. With the gear pump (6), the test tube was flooded with enriched water from the container (15) till a pre-defined water level was reached. This level was monitored by the needle probes (4). After the tube (9) had been uncoupled by switching the three-way-valves (7) and (11), a controlled

expansion of the gas chamber over the water level was realized by the adjustable orifice (13). The release process was initiated by shut-off valve (12). During the release, the system pressure was continuously measured by the pressure transducer (3).

Experiments were carried out for three saturation pressure levels of 30, 50 and 70 bar. The gas release was adjusted to time constants of 6, 12 and 36 s in the case of an exponential approximation of the system pressure course. The test tube was inclined for 15°, 30° and 45°.

3.2.1. Nucleation pressure

The nucleation pressure is defined as the pressure level, where first bubble formation is observed. It is the authors' understanding that the process is dominated by the pressure in first order, which is also represented in the proposed nucleation model.

So far there was no investigation concerning the influence of other parameters for this process.

It is obviously difficult to extract the information when the first nucleation occurs, because there is no chance to observe the liquid in the tube over the full length. So it was decided to define the nucleation pressure at that time, when the first bubble will be detected either by sensor (4) or (5). The authors are aware to underestimate the nucleation pressure slightly by this procedure. But since the transients are slow, the induced error is small.

Observed and simulated values are given in Fig. 12. It can be seen from Fig. 12 that the nucleation pressure is significantly below the saturation pressure. The ratio of these two values is in the order of 2/3. Furthermore, it is obvious that the uncertainty of the experimentally reached values is large. There is no tendency between the release velocity and the nucleation pressure. A good agreement for the prediction of dimension by the simulations is to be seen. A more detailed study of neglected parameters, which alter the nucleation pressure, is the object of further investigations.

3.2.2. Time dependency of the water level

The criterion, which probably is most dominant for practical purpose, is the prediction of the time dependency of the water level. The level changes due to bubble formation and their expansion. In the following, the general behavior as well as sensitivity to different parameters will be discussed.

In general, the water level is defined at the point where the water column reaches the highest value in the z-coordinate. In the case of experiments it was determined by the use of the inductive needle probes. From the time none of the sensors detected water or temporarily gas (bubble), the level was supposed to be higher than the position of this sensor. Vice versa, the level was supposed to be lower if only gas was detected. Since these needle sensors are installed at discrete points, the water level is known at these point on a determined time. Between these times it was linearly interpolated. This linear interpolation results in a smooth appearance of the level curves as it can be seen in Figs. 13 and 15. In the case of simulation, the end of the control volume of highest z-position determines the water level. This value is well known at any time and so there is no requirement for interpolation. If a migrating bubble reaches the surface of the water column, i.e. the time when the LCV had been completely displaced by the rising TPCV, it was defined that the bubble was pushed out of the column immediately. For the next time step, the level was reset to the succeeding LCV taking the amount of water which remained in the TPCV into consideration. This simplification is possible because the amount of water, which a TPCV contains, is comparatively low. Furthermore, any kind of foam formation was neglected due to the same reason. So it is natural that the instantaneous water level does not show the smooth appearance of the experimentally obtained one. From the size of the discontinuities in the course, the length of the pushed out bubbles can be determined.

Table 2
Experimentally determined amount of undissolved gas as a function of saturation pressure

Saturation pressure in bar	30	50	70
Undissolved gas, specific (g/kg)	0.73	1.59	2.73

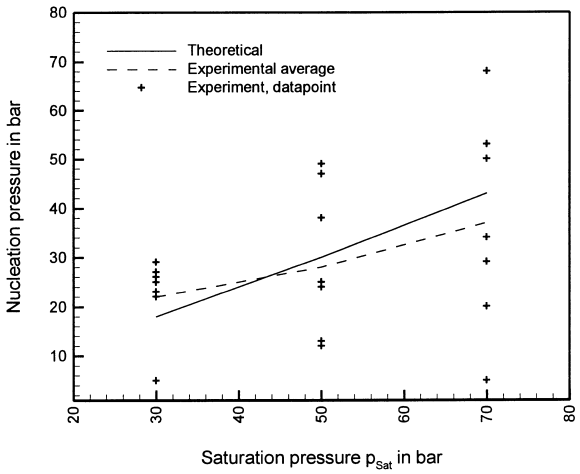

Fig. 12. Nucleation pressure, measured and simulation. The wide range of uncertainty is obvious. The simulated data fit the expected dimension well.

In the first set of depressurization experiments the influence of the inclination angle was investigated. The obtained data are plotted in Fig. 13. It can be seen clearly that the pressure in all three turns behaved approximately exponentially (a time constant was determined for about 13 s). The pressure dropped almost to an atmospheric level after 70 s after the release. Referring to the axis on the right hand side the level course for inclination angles of 15°, 30° and 45° are plotted. For the first 25–30 s the levels increase independently from the nucleation angle. The increase is exponentially and a result of the expansion of micro bubbles. The course of the three levels is similar which is an indicator that the amount of bubbles which left the system was small within these first 25 s (the amount of gas which was not dissolved is similar since it depends only on the saturation pressure, as shown in Table 2). This is natural since the supposed micro bubbles have very slow rising velocity and nucleated bubbles had to be accelerated. After a time period of about 30 s it can be seen that the water level of the configuration with 45° inclination does not show further increase and keeps almost constant for about 30 s. After a short time delay and at higher level maximum the courses of the configuration with 30° and 45° inclination angle behaves similarly. In the case that generation of new volume by nucleation and by expansion of existing bubbles compensates the amount of gas which is continuously pushed out of the system, the formation of a plateau in the level course is yielded. This plateau can clearly be seen in Fig. 13. More inclined tubes cause lower rising velocities of the bubbles and so the amount of bubbles, which reached the surface of the water column within a certain time, is lower. If the amount of gas the system contains, is higher and the pressure is only a function of time, it is clear that the water level increases more as higher as the inclination angle is. Furthermore, the whole course lasts longer with increasing inclination due to slower rising velocities. After about 60 s, the pressure is still about atmospheric, the level decreases slowly since the balance between bubble nucleation and expansion on the one-hand-side and pushed out gas on the other-hand is in non-equilibrium: more gas leaves the column which yields a drop in the water level. This process is as faster as lower the inclination angle is due to increasingly rising velocities. This mechanism is represented by the experiments and can be seen in Fig. 13.

The simulated experiments from Fig. 13 are plotted in Fig. 14. A good agreement can be stated: short plateaus and linear decreases follow an exponential increase of the water levels. The approximate duration of the increase is correctly modeled with about 30 s. The reached maximums are slightly underestimated but reflect the tendency that stronger inclination results in higher values correctly. The duration of the courses as well as their dependence from the inclination angle of the tube is simulated correctly. Besides, it is noteworthy that the released bubbles become larger with increasing time (between 40 and 80 s). This is obvious if the size of the discontinuities in the simulated level course is noticed. Later pushed out bubbles remained longer in the tube which increased the chance of coalescence vehemently. The result is plug formation, which could also be represented by the experiments.

In the second set of depressurization experiments, the influence of a change in the release speed was investigated. Therefore, a fixed configuration with an 45°-inclined test tube was used. The pressure release velocity was varied and the saturation pressure of the

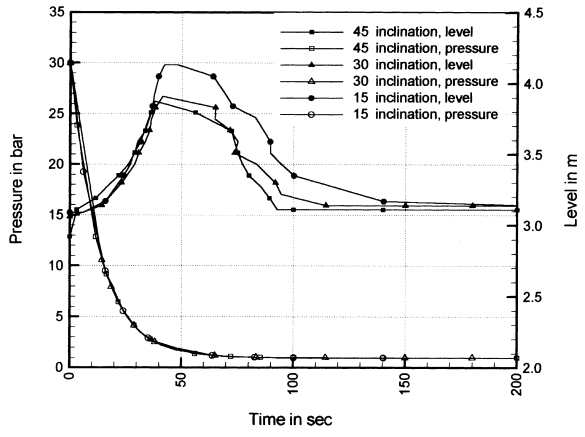

Fig. 13. Level as a function of time. Saturation pressure 30 bar. Pressure gradient with a time constant of $T1 = 13''$. $T = 293$ K.

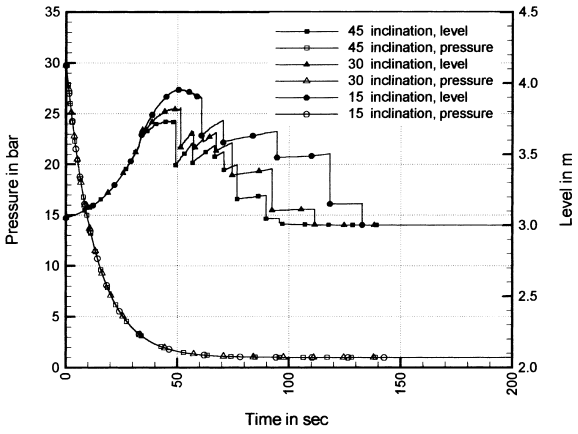

Fig. 14. Simulated level course (like Fig. 13).

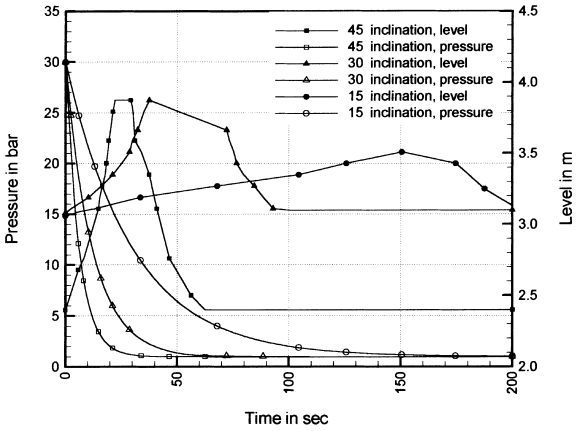

Fig. 15. Level course as a function of tube inclination and saturation pressure.

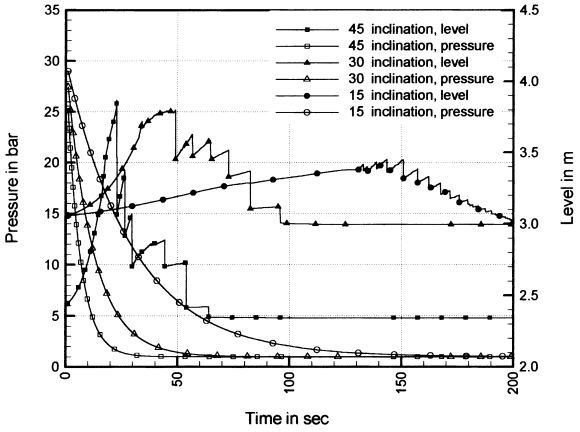

Fig. 16. Simulated level course (like Fig. 15).

dissolved gases was set constant at 30 bar. The reached level courses are illustrated in Fig. 15.

The basic course of the water levels in Fig. 15 is almost the same as in Fig. 13. A fast exponential increase is followed by a plateau with final (linear) decrease. The expansion of the fluid columns in the tube during the first seconds varies since the velocity of the system pressure release is different. The reached plateau values are obviously depending on the velocity of the pressure release. Faster releases yield higher peak values (N.B. that the basic water level of the fastest expansion in Fig. 15 had to be lowered in order to avoid exceeding of the facility's limitations). A faster expansion of the system pressure results in a higher amount of nucleated expanding bubbles, which explains that behavior. This might also be an explanation that the plateaus seem to disappear with increasing release speed. If the pressure drops suddenly, there is no time to develop equilibrium between bubble formation/ expansion and bubble push out since almost all solutes are degassed before larger amounts of bubbles could migrate to the column's surface.

In Fig. 16, it can also be seen that the simulated dependency of the water level course from the velocity of pressure release is represented by the experiments. Increased plateau and decrease of the water levels as well as their dependency on the pressure release speed are simulated correctly. The maximum value is slightly underestimated. The duration of the single processes fits the experimentally reached data well.

It can be stated that the simulations with the proposed model could be verified by the experimental series. The obtained accuracy is good.

4. Conclusion

A one-dimensional flow model is proposed for the simulation of bubbly and plug flow in thin tubes, caused by the depressurization of gas-in-water solutions. The model is based on geometrical assumptions and is valid for junction-less tubing systems of arbitrary inclination. In addition, a bubble nucleation and diffusion model describing the diffusion mass transfer of dissolved gas from the liquid to the bubble, was developed, which can be applied to liquid multi component gas systems.

Separately, the validity of the proposed flow models for the bubble/plug migration was approved by a series of sparkling experiments.

The evidence for the accurate interaction of the three modules (the flow, the nucleation and the diffusion model) is given by nearly authentic representation of the depressurization experiments. The prediction of the onset of nucleation, i.e. the grade of non-equilibrium, was calculated in the right dimension. Furthermore, it is possible to conclude that the diffusion model predicts the right order of mass exchange.

Acknowledgements

The authors express their thanks to Prof. J. Huhn, Dresden University of Technology, Germany, for his advice and encouragement. The project was supported by the Deutsche Forschungsgesellschaft DFG (program: "Transiente Vorgaenge in mehrphasigen Systemen mit einer oder mehreren Komponenten"; item "Ausgasen geloester Gase im Inhaltswasser duenner

Rohrleitungssysteme bei schnellen Druckabsenkungen''; No. SP725).

References

[1] D.J. Tritton, Physical Fluid Dynamics, 2nd ed., Clarendon Press, Oxford, 1987, pp. 48–72.
[2] J.F. Hewitt, N.S. Hall-Taylor, Annular Two-Phase Flow, 1st ed., Pergamon Press, Oxford, 1970, pp. 50–60.
[3] J. Huhn, J. Wolf, Zweiphasenströmung, 1st ed., Fachbuchverlag, Leipzig, 1975.
[4] N.I. Kolev, Transiente Zweiphasenströmung, 1st ed., Springer-Verlag, Berlin, 1986.
[5] M. Ishii, Thermodynamic Theory of Two-Phase Flow, Argonne National Laboratory, Argon, 1963, pp. 14–17.